A new laser–based and ultra–portable gas sensor for indoor and outdoor formaldehyde (HCHO) monitoring

Joshua D. Shutter[1], Norton T. Allen[2], Thomas F. Hanisco[4], Glenn M. Wolfe[4,5], Jason M. St. Clair[4,5], Frank N. Keutsch[1,2,3]

5 [1]Department of Chemistry and Chemical Biology, Harvard University, Cambridge, MA 02138, USA
[2]Harvard John A. Paulson School of Engineering and Applied Sciences, Harvard University, Cambridge, MA 02138, USA
[3]Department of Earth and Planetary Sciences, Harvard University, Cambridge, MA 02138, USA
[4]Atmospheric Chemistry and Dynamics Lab, NASA Goddard Space Flight Center, Greenbelt, MD 20771, USA
[5]Joint Center for Earth Systems Technology, University of Maryland Baltimore County, Baltimore, MD 21228, USA

10 *Correspondence to*: Joshua D. Shutter (shutter@g.harvard.edu)

Abstract. In this work, a new commercially available, laser–based, and ultra–portable formaldehyde (HCHO) gas sensor is characterized, and its usefulness for monitoring HCHO mixing ratios in both indoor and outdoor environments is assessed. Stepped calibrations and intercomparison with well–established laser–induced fluorescence (LIF) instrumentation allow a performance evaluation of the absorption-based, mid–infrared HCHO sensor from Aeris Technologies, Inc. The Aeris sensor

15 displays linear behavior ($R^2 > 0.940$) and shows good agreement with LIF instruments from Harvard and NASA Goddard. A non–linear least–squares fitting algorithm developed independently of the sensor's manufacturer to fit the sensor's raw absorption data during post-processing further improves instrument performance. The 3σ limit of detection (LOD) for a 15 and 60 min integration time is 690 and 420 pptv HCHO, respectively, for mixing ratios reported in real-time, though the LOD improves to 570 and 300 pptv HCHO, respectively, during post-processing. This sub-ppbv precision is sufficient for most HCHO

20 levels measured in indoor and outdoor environments. While the compact Aeris sensor is currently not a replacement for the most sensitive research–grade instrumentation available, its usefulness for monitoring HCHO is clearly demonstrated.

1 Introduction

Understanding the production and lifetime of molecules formed from oxidation chemistry is essential to our understanding of atmospheric chemistry as a whole. Formaldehyde (HCHO) is one of the most ubiquitous tracers of volatile organic compound

25 (VOC) oxidation chemistry since it is generally formed as VOCs are oxidized by compounds such as OH, O_3, and NO_3 (Seinfeld and Pandis, 2016). The measurement of HCHO in situ and via satellite is thus extensively used by models to constrain VOC emissions from both biogenic and anthropogenic sources worldwide and to test our understanding of VOC oxidation chemistry (Choi et al., 2010; Miller et al., 2017; Zhu et al., 2017b).

30 While atmospheric HCHO is primarily produced from the oxidation of VOCs (such as isoprene and CH_4), it is also produced via fuel combustion and biomass burning (Anderson et al., 1996; Holzinger et al., 1999). In the indoor environment, HCHO is released from building materials and cleaning products (Nazaroff and Weschler, 2004), and HCHO mixing ratios are generally higher than those measured outdoors. Normal mixing ratios of HCHO outdoors and indoors can reach upwards of 15 and 40 ppbv, respectively, though elevated levels in both environments can be several times higher (Salthammer, 2013). Given that

35 individuals generally spend ~90% of their time indoors (Klepeis et al., 2001) and that the United States Environmental Protection Agency (US EPA) classifies HCHO as a hazardous air pollutant and probable human carcinogen (Baucus, 1990; U.S. Environmental Protection Agency, 2018), the measurement of HCHO indoors is just as essential as its measurement outdoors. Recently, it has been estimated that 6,600 – 12,000 people in the US will develop cancer over their lifetime due to outdoor

HCHO exposure (Zhu et al., 2017a), which implies that the number from indoor exposure should be substantially higher. The current recommended exposure limit by the National Institute for Occupational Health and Safety (NIOSH) is a time–weighted average of 16 ppbv HCHO for a 10 h workday during a 40 h workweek (Centers for Disease Control and Prevention, 2007).

5 Numerous chemical, spectrometric, and spectroscopic methods have been developed and utilized for the accurate and precise in situ measurement of gas–phase HCHO. Table 1 summarizes several research–grade HCHO instruments developed over the past few decades listing their accuracies as well as limits of detection (3σ) and corresponding integration times. All methods can achieve sub–ppbv detection limits within their specified integration times and accuracies better than or equal to 15%. Of all the methods, the measurement of HCHO by laser–induced fluorescence (LIF) achieves the best detection limit with the shortest
10 integration time. Additionally, chemical derivitization is currently employed as a standard by the US EPA: The current methodology (TO–11A; 2nd ed) for determining HCHO mixing ratios instructs users to sample ambient air with pre–coated DNPH (2,4–dinitrophenylhydrazine) cartridges and then ship these cartridges to a laboratory for analysis of the formaldehyde–DNPH derivative by HPLC (Winberry et al., 1999).

15 Even though these research-grade methods produce high-quality scientific data, they also require large investments of money, power, and operator time. Mass spectrometric methods have high power requirements, are large, are sensitive to humidity effects for the measurement of HCHO, and have possible cross–sensitivities (for any fragment with the same mass–to–charge ratio as ionized HCHO) (Kaiser et al., 2014; Vlasenko et al., 2010). Chemical methods suffer from reproducibility problems at ambient mixing ratios, are labor and time intensive, and require the use of acidic or hazardous reagents. Current laser-based instruments
20 using methods such as LIF, TDLAS, QCLS, and DOAS have sufficient specifications but need knowledgeable operators and are not particularly suitable for widespread adoption in sensor networks. For applications that require a large number of instruments (such as monitoring networks), or the ability to easily and cheaply move instrumentation around from location to location (such as for studying indoor air chemistry), a smaller and easier–to–operate HCHO sensor is preferable that still compares well against research–grade instrumentation with respect to accuracy.

25

Toward this purpose, we characterize a new mid–IR laser–based HCHO sensor (Pico Series) from Aeris Technologies to quantify its performance against some of the best available research–grade instrumentation (i.e., LIF). Through laboratory experiments, the sensor's Allan-Werle deviation curves are calculated to determine the optimal averaging time for HCHO measurements and to assess the sensor's true 3σ limit of detection. The sensor is subsequently compared against LIF
30 instrumentation from NASA and Harvard in the laboratory as a proxy for the sensor's accuracy. Finally, sensor measurements from both outdoor and indoor environments are shown to display the sensor's usefulness for monitoring HCHO.

2 Instrument description

The sensor as supplied has external dimensions of 30 x 20 x 10 cm (11.5 x 8 x 3.75 inches) (Fig. 1), a weight of 3 kg (including batteries), and a proprietary multi–pass detection cell with a volume of 60 cm³ and a 1300 cm path length. The pumping speed is
35 750 standard cubic centimeters per minute (sccm) to maintain a constant pressure of 250 mbar and a residence time of 5 s inside the detection cell. The 6 h battery life, onboard GPS, and 15 W power consumption make the sensor highly portable and thus particularly useful for mobile and field measurements. The sensor is networkable and easy to operate, and HCHO mixing ratios can be monitored via remote desktop over the sensor's Wi–Fi network.

40 Using a proprietary fast-fitting routine that has been optimized to report HCHO and H_2O mixing ratios in real–time (subsequently referred to as the Aeris Real-time (ART) fit), the sensor fits a rovibrational line of HCHO at 2831.6413 cm⁻¹ (with

a corresponding line intensity of $5.839 \cdot 10^{-20}$ cm^{-1} / (molecule $\cdot$ cm^{-2})) that matches the transition chosen by Fried, et al. in their TDLAS system (Fried et al., 1999). A search of the nearby spectral region using the HITRAN database shows this region to be free of strong spectral interferences from other molecular absorbers that would completely prevent the HCHO line from being fit under normal operating conditions (Gordon et al., 2017; Rothman et al., 2013). Additionally, ART fit uses a nearby rovibrational

5 line of an isotopologue of water (HDO) located at 2831.8413 cm^{-1} ($3.014 \cdot 10^{-24}$ cm^{-1} / (molecule $\cdot$ cm^{-2})) as a spectral reference to find and fit the previously mentioned HCHO spectral feature (which the sensor does reliably when H_2O is above 1500 ppmv). The HDO reference line, strongest HCHO spectral feature, and fringes caused by etalons in the optical train are observed in the baseline-subtracted signal depicted in Fig. 2.

10 The raw signal shown in the inset of Fig. 2 is reported at a rate of 1 Hz, and the Beer-Lambert law is used to calculate rudimentary mixing ratios of HCHO and H_2O after baseline subtraction. The sensor also employs a two-inlet design and three-way valve system that allows for the measurement and subtraction of a zero during data collection. Using default settings, the three–way valve cycles between the two inlets at a 50% duty cycle over 30 s. Thus, for 15 s, air flow is directed through the sample inlet, which allows air to directly flow into the detection cell after passing through a particle filter. For the other 15 s, the

15 air flow is directed into the zero inlet containing an inline DNPH cartridge (LpDNPH S10L Cartridge, Sigma–Aldrich) that filters out all aldehydes, including HCHO, from the air flow before it passes through the particle filter and detection cell. Since a zero is effectively calculated every other 15 s with default settings, the inlet and valve setup employed by the sensor helps to minimize the effects of thermal drift and other background effects on the reported HCHO mixing ratio. For instance, since the period of the fringes caused by the etalons in the optical train has a comparable linewidth to the spectral lines being fit, the

20 regular zeroing helps to subtract out the fringes.

The true mixing ratio of HCHO in the sample air over a complete cycle of air flowing through the sample and zero inlets is then defined as the average of the rudimentary 1 Hz HCHO mixing ratios through the sample inlet minus the average of the rudimentary 1 Hz HCHO mixing ratios through the zero inlet for the time period immediately preceding and following the

25 sample inlet:

$$[\text{HCHO}] = \overline{\text{1 Hz Sample Inlet HCHO}} - \left(\frac{\overline{\text{1 Hz Zero Inlet HCHO}_{preceding}} + \overline{\text{1 Hz Zero Inlet HCHO}_{following}}}{2} \right) \tag{1}$$

With this definition, the shortest integration time possible using default settings is 30 s. Equation (1) is subsequently used for all HCHO mixing ratios reported by the Aeris sensor.

30 In this paper, the particle filter was a PTFE filter membrane from Savillex (13 mm ⌀, 1–2 μm pore size). A spectral interference from newly–opened DNPH cartridges was also observed, but this disappears after 2–4 h of continuous sampling. Moreover, the cartridges last anywhere from a few days to a week of continuous use depending on sampling conditions and levels of HCHO encountered.

3 Data processing: Harvard Aeris Post-Processing (HAPP) fit

35 While ART fit is compatible with the sensor's limited on–board computing resources to calculate HCHO mixing ratios in real–time, the sensor also offers the option of outputting its raw 1 Hz spectral data. This raw data was used as input into a repurposed and modified non–linear least–squares fitting program originally developed for the Harvard integrated cavity output spectroscopy (ICOS) instrument (Sayres et al., 2009) in order to extend the fitting capabilities of the sensor and improve the sensor's performance in very dry conditions. Based on the Levenberg–Marquardt algorithm to fit absorption spectra, HAPP fit

includes optional formulations supporting non–linear tuning rates typical of laser photodiodes, standard fits for fixed path length absorption cells, and a variety of options for fitting the baseline power curve and etalons. HAPP fit can dynamically float and fix spectral parameters (within a specified constraint) and group spectral lines of the same species together. Written in C++, the tool is further supported by a suite of MATLAB utilities to assist in setting up the necessary configuration files and exploring the fit
5   results.

Using HAPP fit, several additional HITRAN lines can be fit in addition to the spectral lines used by ART fit. While a full list of fitted spectral lines are provided in Table S1, we notably fit the CH_4 line at 2831.9199 cm^{-1} (1.622·10^{-21} cm^{-1} / (molecule · cm^{-2})). When the absolute water content of the sampled air becomes too low, (i.e., when H_2O < 1500 ppmv – such as during a dry and
10   cold winter) using the previously mentioned HDO line to lock onto the HCHO line becomes impractical. In this case, we found that a small flow (< 1 sccm) of ultra–pure CH_4 (Chemically Pure 99.5% Methane; Airgas) can be added to the inlet line, and the CH_4 line at 2831.9199 cm^{-1} can then be used as a spectral reference to find and fit HCHO at 2831.6413 cm^{-1}. The instrument is considered to run in "CH_4 mode" only when methane is explicitly added to the gas stream; otherwise, the instrument normally uses the water already present in air to run in "HDO mode". CH_4 mode is currently only available in HAPP fit, though a user–
15   controlled software switch between the two modes might be added in a future update of the Aeris sensor.

4 Sensor characterization

4.1 Precision: Allan–Werle deviation and limit of detection (LOD)

The precision of the sensor was calculated for various integration times when running the Aeris sensor in both HDO and CH_4 modes. For HDO mode, a multi–hour zero (20 h) was performed using a tank of ultra–zero air (Airgas). Before the ultra–zero air
20   entered the sensor, the air first passed through a bubbler containing distilled water so that nearly 11,000 ppm H_2O was added to the gas flow. When zeroing the sensor in CH_4 mode for a period of 22 h, a small flow (< 1 sccm) of CH_4 was added to the ultra–zero air. No water was added in CH_4 mode.

Figure 3 shows the Allan–Werle deviation curves for the Aeris sensor in both HDO and CH_4 modes. In HDO mode, HAPP fit
25   outperforms ART fit by nearly 16 ± 9% at all integration times achieving 1σ standard deviations of 800, 190, 100 pptv at a 1, 15, and 60 min integration times, respectively, compared to 1000, 230, and 140 pptv at 1, 15, and 60 min, respectively, for the ART fit. This is unsurprising given that the least squares algorithm in HAPP fit uses more spectral lines than ART fit which uses approximations to display the HCHO mixing ratio in real–time. Additionally, the average of the ART and HAPP HDO fits produces a generally higher precision than either fit individually (700, 660, 180, and 100 pptv at 0.5, 1, 15, and 60 min
30   integration times, respectively). This result has borne out in repeated testing. The difference in precision between HAPP fit and the average of the HDO fits becomes smaller at longer integration times since sensor drift dominates at longer integration times as the true noise averages itself out. Thus, using the average of the two HDO fits, the detection limit of the sensor (3σ) is 540 and 300 pptv at 15 and 60 min, respectively. At essentially all integration times, the precision of HAPP fit in CH_4 mode is lower than the ART HDO fit by a factor of 1.2 ± 0.3, though it must be emphasized that CH_4 mode is the only working mode available
35   during very dry conditions.

4.2 Accuracy: LIF intercomparison

To ascertain the linearity and accuracy of the Aeris sensor in both HDO and CH_4 modes over HCHO mixing ratios commonly measured in outdoor and indoor locations, the Aeris sensor was compared against several LIF HCHO instruments from both Harvard and NASA.

The measurement of HCHO by LIF was first applied to in situ atmospheric measurements by Hottle et al. (2009) using a tunable, Ti:Sapphire laser. Subsequent work by DiGangi, et al. (2011) and Cazorla, et al. (2015) replaced the Ti:Sapphire laser with a narrow–bandwidth fiber laser. In brief, a fiber laser around 353 nm excites a rotational transition in the $4^1_0 A^1 A_2 \leftarrow X^1 A_1$ vibronic

5   band of HCHO, and a photomultiplier tube (PMT) with a long–pass filter measures the resulting fluorescence at wavelengths longer than 370 nm. The mixing ratio of HCHO is proportional to the laser power–normalized PMT counts. This proportionality constant is determined from a known HCHO standard such as a permeation tube or, more recently, a HCHO gas cylinder (Cazorla et al., 2015).

4.2.1 NASA CAFE and ISAF

10   During a HCHO multi–hour intercomparison performed at NASA Goddard in November 2017, the Aeris sensor was operated in HDO mode and compared against NASA LIF instrumentation described previously (Cazorla et al., 2015; operating principle for CAFE described in St. Clair et al., 2017). During this intercomparison, a HCHO gas cylinder (~500 ppbv HCHO balance N_2; Air Liquide) was diluted by an ultra–zero air gas tank to levels between 0 and 25 ppbv HCHO. To the inlet line going to the Aeris sensor, a flow of 158 sccm of humidified ultra–zero air was added to the total flow of 750 sccm so that the HDO line could be

15   used as a reference. All reported values below from the Aeris sensor have already been corrected for this additional dilution factor.

The ART and HAPP fits were compared for the entirety of the intercomparison. Their relationship is shown (with 95% confidence intervals computed) in Eq. (2):

20    $$[\text{HAPP HDO fit}] = (0.98 \pm 0.01) \cdot [\text{ART HDO fit}] - (0.15 \pm 0.14) \tag{2}$$

In general, the HAPP HDO fit computes mixing ratios that are 2% lower (and a negative offset of 150 pptv) than those calculated by ART fit ($R^2 = 0.941$). A correlation plot between the two HDO fits is shown in Fig. S1.

Figure 4 shows correlation plots of the HAPP HDO fit versus the NASA ISAF and CAFE instruments. Figure S2 shows the time

25   series of this same data. All data shown have an integration time of 30 s; the lowest possible integration time for the Aeris at its default settings. With this integration time, the 1σ standard deviation (using the zero air segment) of the Aeris sensor was 1000 pptv while those of NASA ISAF and CAFE were 3 and 40 pptv, respectively. Using a bivariate linear regression fit formulated by York, et al. (2004), Table 2 shows the relationships between the Aeris sensor and NASA LIF instruments. In both comparisons (for which all instruments were independently calibrated), the Aeris instrument calculates mixing ratios that are

30   ~2% higher than the mixing ratios reported by NASA ISAF or CAFE. The Aeris sensor also displays a slight positive offset of 180 to 210 pptv when compared against the NASA instrumentation.

4.2.2 Harvard FILIF

The Aeris sensor was also operated in CH_4 mode and compared against the Harvard FILIF instrument described previously (DiGangi et al., 2011; Hottle et al., 2009) but with several modifications which will be briefly outlined. First, the 32-pass White–

35   type multi–pass detection cell has been replaced with a more stable and easier–to–align single–pass detection cell as described and used in Cazorla, et al. (2015). The single–pass cell is coated in an ultra–black carbon nanotube coating (Singularity Black; NanoLab, Inc.) that minimizes noise in the photomultiplier tube due to scattered photons from the 353 nm laser (NovaWave Technologies, TFL Series). Upgrades to the instrument's electronics and software (now running QNX) have also been performed to increase its reliability as it samples at a default rate of 10 Hz.

This intercomparison utilized a HCHO gas cylinder (600 ppbv HCHO balance N_2; Air Liquide) that was diluted with ultra–zero air (Airgas) to levels between 0 and 50 ppbv HCHO. A check of the mixing ratio of HCHO in the calibration tank was performed using Fourier transform infrared (FTIR) spectroscopy in which HCHO mixing ratios derived from FTIR are scaled by a factor of

5   0.957 in order to tie the calibration to UV cross–sections by Meller and Moortgat (2000) (Cazorla et al., 2015). The scaled FTIR–derived mixing ratio (524 ± 15 ppbv HCHO) was 13% less than what was quoted on the tank, so the scaled FTIR–derived value was used for this comparison. To the 5000 sccm gas flow from the ultra–zero air tank, < 1 sccm of ultra–pure CH_4 (Chemically Pure 99.5% Methane; Airgas) was added so that the Aeris sensor was running in CH_4 mode.

10   Figure 5 shows the results of the multi–day stepped intercomparison between Harvard FILIF and the Aeris sensor. In the first non-zero HCHO step, both the Aeris sensor and Harvard FILIF instrument show that the HCHO mixing ratio took several hours to stabilize at 15.3 ppbv. This is likely due to the HCHO gas passivating the stainless–steel surfaces of the gas regulator and MKS mass flow controller (500 sccm full scale) even though the latter was coated in a FluoroPel omniphobic coating (FluoroPel 800; Cytonix). All other surfaces were PFA plastic. This highlights the need to perform HCHO calibrations over several hours to

15   allow for passivation of all surfaces.

At 30 s, the Aeris sensor had a 1σ precision of 1350 pptv as opposed to 22 pptv for Harvard FILIF during this experiment. The difference does improve at a 1 h integration time when the 1σ precision for the Aeris becomes 230 pptv and that of FILIF is 8.5 pptv. Table 2 shows the results of a linear regression of the HCHO mixing ratios from the Aeris sensor versus those reported by

20   Harvard FILIF. The regression shows the Aeris sensor reporting the HCHO mixing ratio as ~1% higher when compared to FILIF with a negative offset of 150 pptv. These results obtained with a different calibration tank and different LIF instrument are in excellent agreement with the ones obtained during the intercomparison at NASA Goddard, demonstrating the good accuracy and linearity of the Aeris sensor even at low mixing ratios.

5 Outdoor and indoor ambient measurements

25   The Aeris sensor and Harvard FILIF were collocated in Cambridge, MA to sample outdoor air for several days at the end of June 2018. The ART and HAPP fit hourly averages for HCHO in HDO mode are compared against the mixing ratios from Harvard FILIF in Fig. 6. Though conditions during the measurement period were generally partly or mostly cloudy with highs reaching 33°C by the end of the week, it was punctuated by rain showers that lasted from the evening of June 27 to the evening of June 28. During this time, both ART and HAPP fit HCHO underpredicted FILIF by ~500 pptv, though this is a sampling error due to

30   water condensing onto the optics of the sensor (as evidenced by some slight water damage observed on the optical coating following this experiment). This problem can be alleviated in the future with an inline water trap and ensuring that the sensor is not substantially colder than the temperature of the ambient air.

Considering all hours except for the rain showers (n = 62 h), 87% of the HAPP fit hourly mixing ratios are within ±0.5 ppbv of

35   FILIF and 100% are within ±1 ppbv. Similarly, 74% and 98% of the ART fit hourly mixing ratios are within ±0.5 and ±1 ppbv of FILIF, respectively. Table 3 shows the results of a linear regression of ART and HAPP fit HCHO mixing ratios versus those reported by FILIF. The regression demonstrates that the ART fit mixing ratios were ~7% lower than FILIF with a positive offset of 390 pptv. On the other hand, the HAPP fit mixing ratios were ~7% higher than FILIF with a negative offset of 200 pptv. With both fits within ±10% of FILIF, these results readily demonstrate the utility of using the Aeris sensor as a monitor for ambient

40   levels of HCHO in the environment.

The portability of the Aeris sensor was also demonstrated by carrying it as a personal HCHO exposure monitor over a period of several hours on and around the Harvard campus. Figure 7 shows a map of the locations visited. Even though the data was collected during a winter month in Massachusetts when the air is generally cold and dry (which would necessitate running in CH_4 mode), the sensor operated in HDO mode due to an unseasonal local temperature of 22°C and 63% relative humidity. The

5   sensor's batteries did not have to be recharged during the measurement period.

The five measurement sites (with two–min averaged, HAPP HDO fit HCHO mixing ratios and 1σ standard deviation of measured values in parentheses) were (A) an office space (9.73 ± 0.86 ppbv), (B) an urban park (-0.2 ± 1.2 ppbv), (C) a cafeteria during lunchtime (7.00 ± 0.94 ppbv), (D) the ant collection room in the Harvard Natural History Museum (17.9 ± 1.6 ppbv), and

10   (E) laboratory space in the Mallinckrodt Chemistry Building (4.87 ± 1.13 ppbv). All locations were indoors except for B. This sampling demonstrates the portability of the sensor in both indoor and outdoor locations. Even though the LIF instruments have much higher precision than the Aeris sensor, this simple experiment around the Harvard campus would be cumbersome and logistically impractical given the size and power requirements of the LIF instruments and other spectroscopic and spectrometric methods mentioned previously. Moreover, all the mixing ratios were calculated in real–time unlike offline HCHO measurement

15   methods such as the current EPA standard methodology.

6 Conclusions

While the Aeris sensor is not a replacement for research–grade instrumentation for measuring HCHO in some applications, its ease–of–use, portability, and cost make the sensor a prime candidate for use in a variety of routine monitoring applications. The 3σ limit of detection at a 15 min integration time is 690 and 570 pptv HCHO for ART and HAPP fits, respectively, which

20   improves to 420 and 300 pptv HCHO at a 60 min integration time. With sub-ppbv precision at these times, the sensor can easily distinguish between ambient levels of HCHO normally found in outdoor and indoor locations. Moreover, the ambient outdoor air intercomparison with Harvard FILIF in Fig. 6 shows that the Aeris sensor hourly HCHO is generally within ±0.5 ppbv of the HCHO mixing ratio reported by LIF instrumentation. This intercomparison demonstrates that the sensor is a viable alternative for ambient air monitoring networks or perhaps indoor air chemistry studies. However, in its current state, the sensor is not

25   suitable for eddy–covariance flux measurements which require a much faster time resolution and precision than what the sensor currently provides.

As discussed in the text, the sensor can operate in both HDO and CH_4 mode. While HDO mode is preferable in most cases, during cold weather operation when the air is dry, it is recommended to run the Aeris sensor in CH_4 mode by adding a < 1 sccm

30   flow from an ultra–pure CH_4 gas tank. While this makes the sensor less portable, it ensures that data can still be collected in these conditions. The need for a spare CH_4 gas tank would be made obsolete if a small CH_4 reference cell were added to the sensor or the etalons were reduced or better characterized by software to improve the signal–to–noise ratio on the HDO spectral line.

Code and data availability

HAPP fit can be provided upon request by email to Norton T. Allen (allen@huarp.harvard.edu) or via GitHub

35   (https://github.com/nthallen/le-icosfit). Data used in this paper can be provided upon request by email to Joshua D. Shutter (shutter@g.harvard.edu).

Author contributions

JDS led this work, designed and carried out experiments, completed the data analysis, and wrote the paper with input from all co-authors. NTA wrote HAPP fit and assisted JDS with data analysis. TFH oversees all NASA LIF instrumentation and approved intercomparison efforts at NASA Goddard. GMW provided data from NASA ISAF and designed experiments during the NASA

5 Goddard intercomparison in November-December 2017. JMSC provided data from NASA CAFE. As principal investigator, FNK provided supervision and acquired financial support for this project.

Competing interests

The authors declare that they have no conflict of interest.

Acknowledgements

10 The authors acknowledge Aeris Technologies (Joshua B. Paul, Jerome Thiebaud, Stephen So, and James J. Scherer) for helpful discussions along with the development and fabrication of the sensor. Additionally, the authors acknowledge Joshua L. Cox for his assistance during the HCHO intercomparison at NASA Goddard in November–December 2017. This material is based upon work supported by the National Science Foundation Graduate Research Fellowship under Grant No. DGE–1745303.

References

15 Anderson, L. G., Lanning, J. A., Barrell, R., Miyagishima, J., Jones, R. H. and Wolfe, P.: Sources and sinks of formaldehyde and acetaldehyde: An analysis of Denver's ambient concentration data, Atmos. Environ., 30(12), 2113–2123, doi:10.1016/1352-2310(95)00175-1, 1996.

Baucus, M.: S. 1630 - 101st Congress: Clean Air Act Amendments of 1990, United States Congress, Washington, DC., 1990.

Cazorla, M., Wolfe, G. M., Bailey, S. A., Swanson, A. K., Arkinson, H. L. and Hanisco, T. F.: A new airborne laser-induced

20 fluorescence instrument for in situ detection of formaldehyde throughout the troposphere and lower stratosphere, Atmos. Meas. Tech., 8(2), 541–552, doi:10.5194/amt-8-541-2015, 2015.

Centers for Disease Control and Prevention: NIOSH Pocket Guide to Chemical Hazards, [online] Available from: https://www.cdc.gov/niosh/npg/npgd0293.html (Accessed 30 September 2018), 2007.

Choi, W., Faloona, I. C., Bouvier-Brown, N. C., McKay, M., Goldstein, A. H., Mao, J., Brune, W. H., LaFranchi, B. W., Cohen,

25 R. C., Wolfe, G. M., Thornton, J. A., Sonnenfroh, D. M. and Millet, D. B.: Observations of elevated formaldehyde over a forest canopy suggest missing sources from rapid oxidation of arboreal hydrocarbons, Atmos. Chem. Phys., 10(18), 8761–8781, doi:10.5194/acp-10-8761-2010, 2010.

St. Clair, J. M., Swanson, A. K., Bailey, S. A., Wolfe, G. M., Marrero, J. E., Iraci, L. T., Hagopian, J. G. and Hanisco, T. F.: A new non-resonant laser-induced fluorescence instrument for the airborne in situ measurement of formaldehyde, Atmos. Meas.

30 Tech., 10(12), 4833–4844, doi:10.5194/amt-10-4833-2017, 2017.

DiGangi, J. P., Boyle, E. S., Karl, T., Harley, P., Turnipseed, A., Kim, S., Cantrell, C., Maudlin, R. L., Zheng, W., Flocke, F., Hall, S. R., Ullmann, K., Nakashima, Y., Paul, J. B., Wolfe, G. M., Desai, A. R., Kajii, Y., Guenther, A. and Keutsch, F. N.: First direct measurements of formaldehyde flux via eddy covariance: Implications for missing in-canopy formaldehyde sources, Atmos. Chem. Phys., 11(20), 10565–10578, doi:10.5194/acp-11-10565-2011, 2011.

35 Fried, A., Wert, B. P., Henry, B. and Drummond, J. R.: Airborne tunable diode laser measurements of formaldehyde, Spectrochim. Acta Part A Mol. Biomol. Spectrosc., 55(10), 2097–2110, doi:10.1016/S1386-1425(99)00082-7, 1999.

Gordon, I. E., Rothman, L. S., Hill, C., Kochanov, R. V., Tan, Y., Bernath, P. F., Birk, M., Boudon, V., Campargue, A., Chance, K. V., Drouin, B. J., Flaud, J.-M., Gamache, R. R., Hodges, J. T., Jacquemart, D., Perevalov, V. I., Perrin, A., Shine, K. P., Smith, M.-A. H., Tennyson, J., Toon, G. C., Tran, H., Tyuterev, V. G., Barbe, A., Császár, A. G., Devi, V. M., Furtenbacher, T., Harrison, J. J., Hartmann, J.-M., Jolly, A., Johnson, T. J., Karman, T., Kleiner, I., Kyuberis, A. A., Loos, J., Lyulin, O. M.,

5 Massie, S. T., Mikhailenko, S. N., Moazzen-Ahmadi, N., Müller, H. S. P., Naumenko, O. V., Nikitin, A. V., Polyansky, O. L., Rey, M., Rotger, M., Sharpe, S. W., Sung, K., Starikova, E., Tashkun, S. A., VanderAuwera, J., Wagner, G., Wilzewski, J., Wcisło, P., Yu, S. and Zak, E. J.: The HITRAN2016 molecular spectroscopic database, J. Quant. Spectrosc. Radiat. Transf., 203, 3–69, doi:10.1016/J.JQSRT.2017.06.038, 2017.

Holzinger, R., Warneke, C., Hansel, A., Jordan, A., Lindinger, W., Scharffe, D. H., Schade, G. and Crutzen, P. J.: Biomass

10 burning as a source of formaldehyde, acetaldehyde, methanol, acetone, acetonitrile, and hydrogen cyanide, Geophys. Res. Lett., 26(8), 1161–1164, doi:10.1029/1999GL900156, 1999.

Hottle, J. R., Huisman, A. J., DiGangi, J. P., Kammrath, A., Galloway, M. M., Coens, K. L. and Keutsch, F. N.: A laser induced fluorescence-based instrument for in-situ measurements of atmospheric formaldehyde, Environ. Sci. Technol., 43(3), 790–795, doi:10.1021/es801621f, 2009.

15 Kaiser, J., Li, X., Tillmann, R., Acir, I., Holland, F., Rohrer, F., Wegener, R. and Keutsch, F. N.: Intercomparison of Hantzsch and fiber-laser-induced-fluorescence formaldehyde measurements, Atmos. Meas. Tech., 7(6), 1571–1580, doi:10.5194/amt-7-1571-2014, 2014.

Klepeis, N. E., Nelson, W. C., Ott, W. R., Robinson, J. P., Tsang, A. M., Switzer, P., Behar, J. V, Hern, S. C. and Engelmann, W. H.: The National Human Activity Pattern Survey (NHAPS): A resource for assessing exposure to environmental pollutants, J.

20 Expo. Sci. Environ. Epidemiol., 11(3), 231–252, doi:10.1038/sj.jea.7500165, 2001.

MapTiler and OpenStreetMap Contributors: Maputnik v1.5.0, [online] Available from: https://www.openstreetmap.org, https://openmaptiles.org, and https://maputnik.github.io, 2018. OpenStreetMap data is available under the Open Database License and cartography is licensed as CC BY-SA.

McManus, J. B., Zahniser, M. S., Nelson, D. D., Shorter, J. H., Herndon, S. C., Wood, E. C. and Wehr, R.: Application of

25 quantum cascade lasers to high-precision atmospheric trace gas measurements, Opt. Eng., 49(11), 111124, doi:10.1117/1.3498782, 2010.

Meller, R. and Moortgat, G. K.: Temperature dependence of the absorption cross sections of formaldehyde between 223 and 323 K in the wavelength range 225-375 nm, J. Geophys. Res. Atmos., 105(D6), 7089–7101, doi:10.1029/1999JD901074, 2000.

Miller, C. C., Jacob, D. J., Marais, E. A., Yu, K., Travis, K. R., Kim, P. S., Fisher, J. A., Zhu, L., Wolfe, G. M., Hanisco, T. F.,

30 Keutsch, F. N., Kaiser, J., Min, K. E., Brown, S. S., Washenfelder, R. A., González Abad, G. and Chance, K.: Glyoxal yield from isoprene oxidation and relation to formaldehyde: Chemical mechanism, constraints from SENEX aircraft observations, and interpretation of OMI satellite data, Atmos. Chem. Phys., 17(14), 8725–8738, doi:10.5194/acp-17-8725-2017, 2017.

Nazaroff, W. W. and Weschler, C. J.: Cleaning products and air fresheners: Exposure to primary and secondary air pollutants, Atmos. Environ., 38(18), 2841–2865, doi:10.1016/J.ATMOSENV.2004.02.040, 2004.

35 Rothman, L. S., Gordon, I. E., Babikov, Y., Barbe, A., Benner, D. C., Bernath, P. F., Birk, M., Bizzocchi, L., Boudon, V., Brown, L. R., Campargue, A., Chance, K., Cohen, E. A., Coudert, L. H., Devi, V. M., Drouin, B. J., Fayt, A., Flaud, J.-M., Gamache, R. R., Harrison, J. J., Hartmann, J.-M., Hill, C., Hodges, J. T., Jacquemart, D., Jolly, A., Lamouroux, J., Le Roy, R. J., Li, G., Long, D. A., Lyulin, O. M., Mackie, C. J., Massie, S. T., Mikhailenko, S., Müller, H. S. P., Naumenko, O. V., Nikitin, A. V., Orphal, J., Perevalov, V., Perrin, A., Polovtseva, E. R., Richard, C., Smith, M. A. H., Starikova, E., Sung, K., Tashkun, S.,

40 Tennyson, J., Toon, G. C., Tyuterev, V. G. and Wagner, G.: The HITRAN2012 molecular spectroscopic database, J. Quant. Spectrosc. Radiat. Transf., 130, 4–50, doi:10.1016/j.jqsrt.2013.07.002, 2013.

Salthammer, T.: Formaldehyde in the ambient atmosphere: From an indoor pollutant to an outdoor pollutant?, Angew. Chemie

Int. Ed., 52(12), 3320–3327, doi:10.1002/anie.201205984, 2013.

Sayres, D. S., Moyer, E. J., Hanisco, T. F., St Clair, J. M., Keutsch, F. N., O'Brien, A., Allen, N. T., Lapson, L., Demusz, J. N., Rivero, M., Martin, T., Greenberg, M., Tuozzolo, C., Engel, G. S., Kroll, J. H., Paul, J. B. and Anderson, J. G.: A new cavity based absorption instrument for detection of water isotopologues in the upper troposphere and lower stratosphere, Rev. Sci.

5 Instrum., 80(4), 044102, doi:10.1063/1.3117349, 2009.

Seinfeld, J. H. and Pandis, S. N.: Atmospheric Chemistry and Physics: From Air Pollution to Climate Change, 3rd ed., Wiley., 2016.

U.S. Environmental Protection Agency: Risk Assessment for Carcinogenic Effects, 2018.

Vlasenko, A., Macdonald, A. M., Sjostedt, S. J. and Abbatt, J. P. D.: Formaldehyde measurements by Proton transfer reaction -

10 Mass spectrometry (PTR-MS): Correction for humidity effects, Atmos. Meas. Tech., 3(4), 1055–1062, doi:10.5194/amt-3-1055-2010, 2010.

Weibring, P., Richter, D., Walega, J. G. and Fried, A.: First demonstration of a high performance difference frequency spectrometer on airborne platforms, Opt. Express, 15(21), 13476–13495, doi:10.1364/OE.15.013476, 2007.

Winberry, W. T., Tejada, S., Lonneman, B. and Kleindienst, T.: Compendium of Methods for the Determination of Toxic

15 Organic Compounds in Ambient Air: Compendium Method TO-11A, 2nd ed., U.S. Environmental Protection Agency, Cincinnati, OH., 1999.

Wisthaler, A., Apel, E. C., Bossmeyer, J., Hansel, A., Junkermann, W., Koppmann, R., Meier, R., Müller, K., Solomon, S. J., Steinbrecher, R., Tillmann, R. and Brauers, T.: Technical Note: Intercomparison of formaldehyde measurements at the atmosphere simulation chamber SAPHIR, Atmos. Chem. Phys., 8(8), 2189–2200, doi:10.5194/acp-8-2189-2008, 2008.

20 York, D., Evensen, N. M., Martínez, M. L. and De Basabe Delgado, J.: Unified equations for the slope, intercept, and standard errors of the best straight line, Am. J. Phys., 72(3), 367–375, doi:10.1119/1.1632486, 2004.

Zhu, L., Jacob, D. J., Keutsch, F. N., Mickley, L. J., Scheffe, R., Strum, M., González Abad, G., Chance, K., Yang, K., Rappenglück, B., Millet, D. B., Baasandorj, M., Jaeglé, L. and Shah, V.: Formaldehyde (HCHO) as a hazardous air pollutant: Mapping surface air concentrations from satellite and inferring cancer risks in the United States, Environ. Sci. Technol., 51(10),

25 5650–5657, doi:10.1021/acs.est.7b01356, 2017a.

Zhu, L., Mickley, L. J., Jacob, D. J., Marais, E. A., Sheng, J., Hu, L., Abad, G. G. and Chance, K.: Long-term (2005–2014) trends in formaldehyde (HCHO) columns across North America as seen by the OMI satellite instrument: Evidence of changing emissions of volatile organic compounds, Geophys. Res. Lett., 44(13), 7079–7086, doi:10.1002/2017GL073859, 2017b.

30

35

40

Table 1. Overview of selected in situ HCHO measurement techniques

	Method	3σ Limit of Detection (pptv)	Integration Time (s)	Accuracy (%)	Reference
Chemical	Fluorimetry[a] (Enzymatic and Hantzsch)	75–120	60–120	5–8	(Kaiser et al., 2014; Wisthaler et al., 2008)
	DNPH–HPLC	60	3600	15	(Wisthaler et al., 2008)
Spectroscopy/Spectrometry	Proton Transfer Reaction–Mass Spectrometry (PTR–MS)	300	2	10	(Wisthaler et al., 2008)
	Tunable Diode Laser Absorption Spectroscopy (TDLAS)	180	1	6	(Fried et al., 1999; Weibring et al., 2007)
	Quantum Cascade Laser Spectroscopy (QCLS)	96	1	–	(McManus et al., 2010)
	Differential Optical Absorption Spectroscopy (DOAS)	600	100	6	(Wisthaler et al., 2008)
	Laser–Induced Fluorescence (LIF)	30	1	10	(Cazorla et al., 2015; St. Clair et al., 2017; DiGangi et al., 2011; Hottle et al., 2009)

[a]Specified values are for Hantzsch

Figure 1. Internal view of the mid–IR, laser–based HCHO sensor from Aeris Technologies. The sensor fits inside a Pelican case that provides for easy transport and mobility.
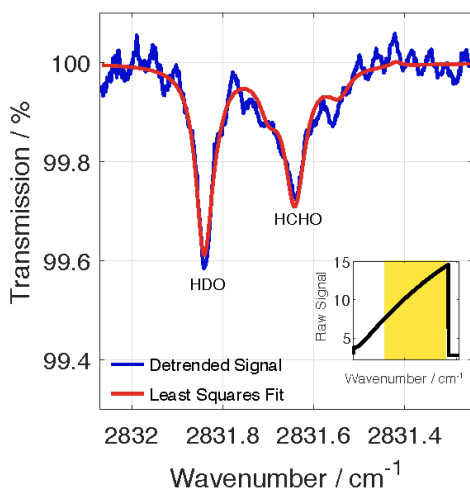
Figure 2. When the H_2O mixing ratio is above 1500 ppmv, the HDO line at 2831.8413 cm^{-1} rises above the fringing caused by etalons in the detection cell so that the position of the HCHO line at 2831.6413 cm^{-1} can be reliably located and the spectral line fit. The fit depicted corresponds to a HCHO mixing ratio around 800 ppbv. (*inset*) 1 Hz raw data from the sensor before baseline subtraction. The yellow shaded region corresponds to the wavelength range being fit.
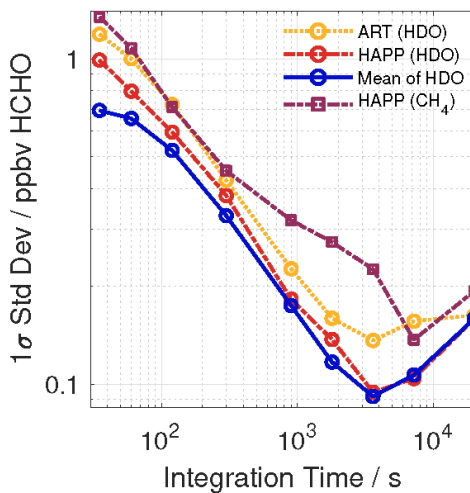
Figure 3. Allan–Werle deviation curves HCHO measurements by the Aeris sensor with different fitting modes. In HDO mode, ART and HAPP fits are shown as well as their mean. In CH_4 mode, the HAPP fit is shown. The average of the ART and HAPP fits in HDO mode produces the lowest 1σ standard deviation with a minimum of 100 pptv for a 1 h integration time. Table S2 lists 1σ standard deviations at selected integration times.
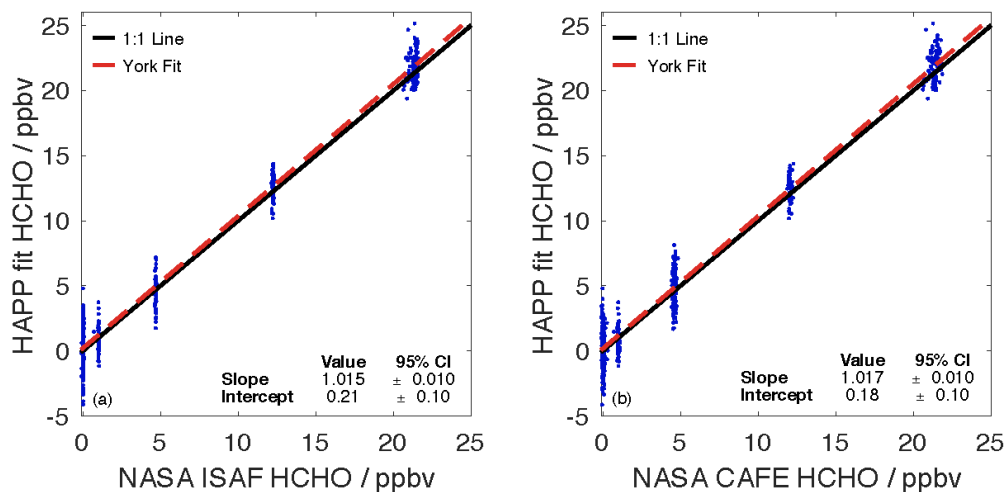
Figure 4. Correlation plots between the HAPP fit and two NASA LIF instruments: (a) NASA ISAF ($R^2 = 0.979$) and (b) NASA CAFE ($R^2 = 0.976$). A time series plot for the stepped intercomparison performed at NASA Goddard is located in the supplemental information (Fig. S2).
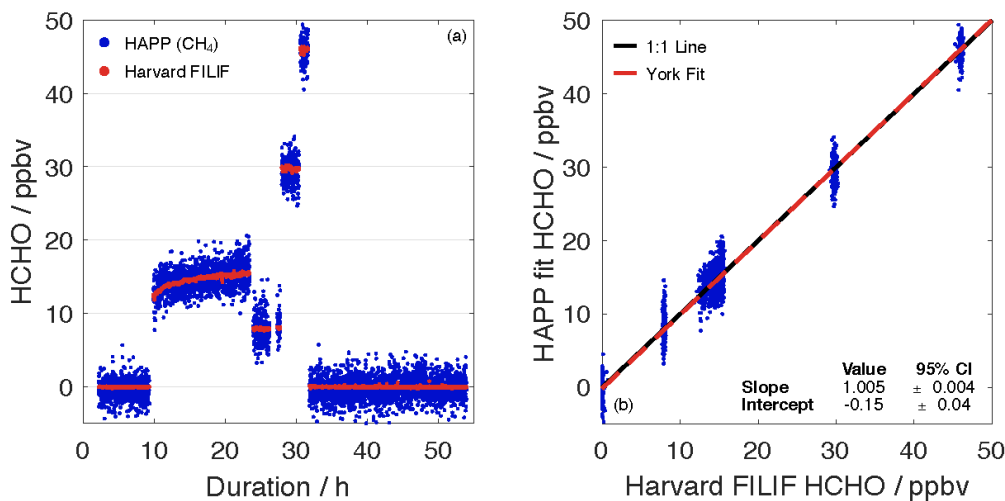
Figure 5. (a) Time series of the Aeris sensor (HAPP CH_4 fit) and Harvard FILIF during a multi–day stepped intercomparison. All data are reported with an integration time of 30 s. (b) Correlation plot between the Aeris sensor (HAPP CH_4 fit) and Harvard FILIF ($R^2 = 0.980$).

Table 2. Regression analyses for Aeris sensor vs LIF instruments calculated with a 95% confidence interval

		Linear Fit ($[Aeris] = m \cdot [LIF\ instrument] + b$)		
	Sensor Mode	m	b	R^2
NASA ISAF	HDO	1.015 ± 0.010	0.21 ± 0.10	0.979
NASA CAFE	HDO	1.017 ± 0.010	0.18 ± 0.10	0.976
Harvard FILIF	CH_4	1.005 ± 0.004	-0.15 ± 0.04	0.980

Bivariate least squares regressions were calculated according to the method of York, et al (2004). HAPP fits were used for reporting the HCHO mixing ratio from the Aeris sensor. Units are in ppbv.
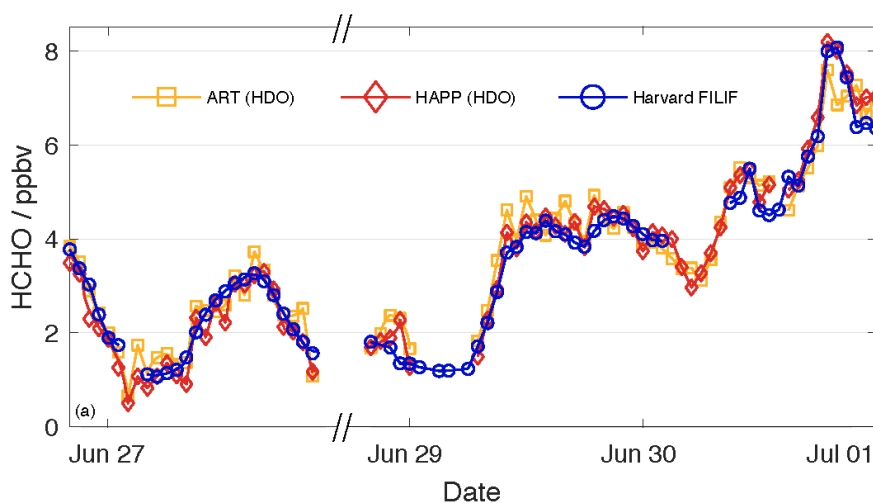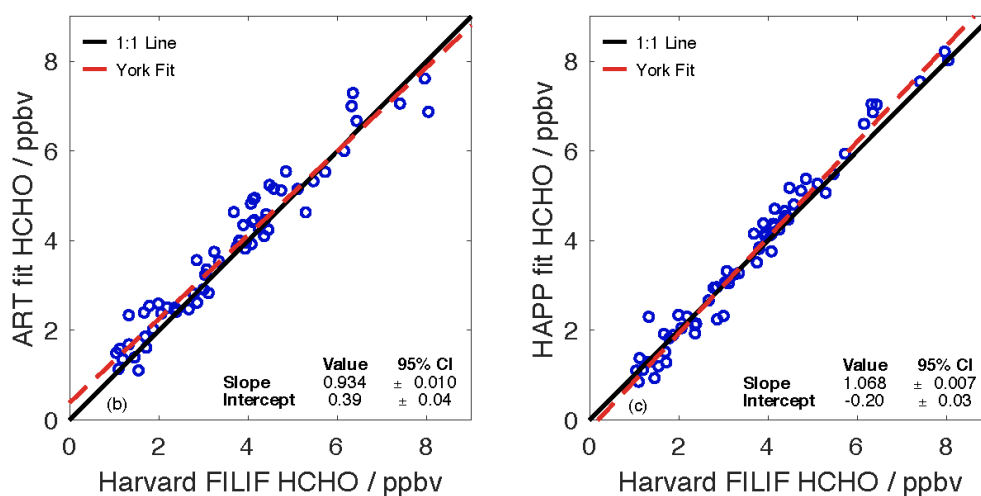
Figure 6. (a) Collocated, multi–day sampling of ambient air in Cambridge, MA, by Harvard FILIF and the Aeris sensor (HDO mode). Ticks represent midnight (00:00) on the specified date. All data is reported with an integration time of 60 min. From the evenings of June 27–28, the area experienced rain showers that caused both the ART and HAPP fits to underestimate the HCHO mixing ratio by ~0.5 ppbv due to water condensing on the optics. Data from the Aeris sensor
10   was also removed (1) during the early hours of June 29 due to replacement of the DNPH cartridge and (2) during the afternoon of June 30 due to zeroing of the sensor with ultra-zero air. Correlation plots comparing Harvard FILIF with (b) ART fit ($R^2 = 0.940$) and (c) HAPP fit ($R^2 = 0.974$).

Table 3. Regression analysis for Aeris sensor vs Harvard FILIF sampling ambient air calculated with a 95% confidence interval

	Linear Fit ($[Aeris] = m \cdot [Harvard \; FILIF] + b$)		
	m	b	R^2
ART fit	0.934 ± 0.010	0.39 ± 0.04	0.940
HAPP fit	1.068 ± 0.007	-0.20 ± 0.03	0.974

Bivariate least squares regressions were calculated according to the method of York, et al (2004). Units are in ppbv.
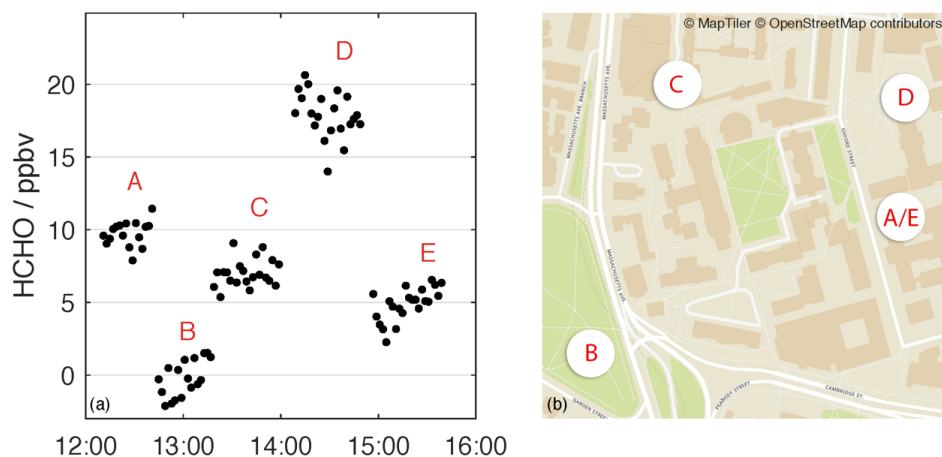
5   Figure 7. (a) Aeris sensor (operating in HDO mode) used as a HCHO personal exposure monitor for several hours on a single battery charge around the Harvard campus in Cambridge, MA. All times EDT. Locations included (A) office space, (B) urban park, (C) cafeteria, (D) museum space, and (E) lab space. The data from HAPP fit is displayed with an integration time of 2 min. Data is not shown when the sensor was transported from one location to another. (b) Map data © OpenStreetMap contributors. Schema from OpenMapTiles.org (MapTiler and OpenStreetMap Contributors, 2018).